ACS APPLIED MATERIALS & INTERFACES

Research Article

www.acsami.org

Ultrasound-Triggered BSA/SPION Hybrid Nanoclusters for Liver-Specific Magnetic Resonance Imaging

Bingbo Zhang,*[,†] Qi Li,[‡] Peihao Yin,[‡] Yuanpeng Rui,[§] Yanyan Qiu,[‡] Yan Wang,[‡] and Donglu Shi*[,†,∥]

[†]The Institute for Biomedical Engineering & Nano Science, Tongji University School of Medicine, Shanghai, 200092, P. R. China

[‡]Department of Clinical Oncology , Putuo Hospital, Shanghai University of Traditional Chinese Medicine, Shanghai, 200062, P. R. China

[§]Medical Imaging Center, Putuo Hospital, Shanghai University of Traditional Chinese Medicine, Shanghai, 200062, P. R. China

[∥]School of Electronic and Computing Systems, University of Cincinnati, Cincinnati, Ohio 45221, United States

ABSTRACT: Nanoclusters of superparamagnetic iron oxide nanoparticles (SPION) are developed for liver-specific magnetic resonance imaging (MRI) by a unique synthesis route. The process is efficient, environmentally benign, and straight forward within five minutes. The clustering effect is triggered in the presence of bovine serum albumin (BSA) aqueous phase under ultrasonication condition. The hydrophobic SPION are densely self-assembled into BSA/SPION hybrid nanoclusters with a uniform size of ~86 nm. The as-prepared BSA/SPION hybrid nanoclusters are found to be biocompatible and stable. They exhibit high transverse relaxivity and longitudinal relaxivity in water (r_2 and r_1 values are 600.8 and 4.3 s^{-1} per mM of Fe^{3+}, respectively). In vivo T_2-weighted MRI shows excellent enhancement in liver with an imaging time-window up to 48 h. In vivo biodistribution study indicates a gradual excretion of the nanoclusters via hepatobiliary (HB) processing. No toxicity is observed in the in vivo and ex vivo experiments. The BSA/SPION hybrid nanoclusters present great potential in MRI as the liver-specific contrast agents (CAs).

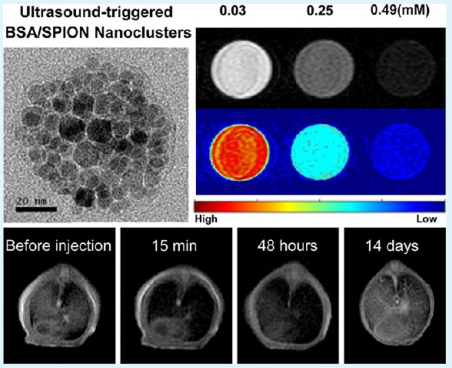

KEYWORDS: *iron oxide, bovine serum albumin, ultrasound, magnetic resonance imaging, liver*

1. INTRODUCTION

Magnetic resonance imaging (MRI) has been commonly used for medical diagnosis.[1−5] The MRI technique offers non-invasive assessment of tissues in terms of both anatomy and function.[6,7] However, current clinical contrast agents (CAs) are not satisfactorily sufficient for liver-specific MRI. For instance, Gd-DTPA (magnevist, trade name), as one of the frequently used CAs, can be rapidly excreted from body via renal metabolism.[8] In this situation, the time-window for liver scanning is too narrow for accurate imaging. Furthermore, Gd-DTPA has been reported to be toxic that is particularly harmful to kidneys.[9] There is, therefore, a great need to search for biocompatible liver−specific MRI CAs with a large imaging time-window and gradual excretion.

Superparamagnetic iron oxide nanoparticles (SPION) have been extensively reported as liver MRI CAs because they are strong enhancers of proton relaxation with superior MR T_2 (transverse relaxation) shortening effects.[10−12] SPION are also known for their good biocompatibility. In liver MRI, SPION can preferentially be taken up by macrophages in the liver for a period of time and excreted gradually via hepatobiliary (HB) processing.[13] Its gadolinium-based counterpart is, however, not only reported toxic but rapidly cleared from body because of low molecular weight.[9]

It has been reported that the transverse relaxivity can be significantly increased by clustering of individual SPION.[14] Berret et al. found that the transverse relaxivity was noticeably increased by the magnetic clusters in the range of 70−150 nm.[15] Similar results were also reported by Zhang et al.[16] As such, several techniques based on clustering of SPION have been developed.[17−19] The "oil-in-water" micelles method is one of the most frequently used approaches for preparation of nanoclusters.[14,17,20−22] This method involves adding the hydrophobic SPION/amphiphilic polymer organic phase into water while stirring. Although amphiphilic polymers can be artificially synthesized, the processing is not easily and accurately controlled. As a consequence, the resulting amphiphilic polymers exhibit heterogeneity from different batches. Furthermore, the chemical synthesis of amphiphilic polymers is tedious, high cost, and environmentally unfriendly.

In this study, an alternative strategy was developed based on the principle of the "oil-in-water" method. Bovine serum albumin (BSA) protein was selected as the SPION stabilizer polymer, which is commercially available. BSA is a zwitterionic surfactant with abundant carboxyl and amino groups. It can

Received: July 11, 2012
Accepted: November 14, 2012
Published: November 14, 2012

foam easily in water by action of vigorous stirring or ultrasonication.[23,24] Thus, it can be used as an emulsifying agent. BSA is also the principal carrier of fatty acids that are otherwise insoluble in circulating plasma.[25] It is reported that albumin has a high affinity for hydrophobic fatty acids, hematin, bilirubin, and a broad affinity for small aromatic compounds.[26−29] In this study, SPION were coated with hydrophobic fatty acids, and bonded with BSA proteins. The clustering of SPION was initiated as a result of bonding under ultrasonication in the presence of BSA. The clustering process is facile, environmentally benign, reproducible, and rapid within 5 minutes. The as-prepared BSA/SPION hybrid nanoclusters exhibit good colloidal stability, high r_2 relaxivity, and pronounced liver-specific MRI.

2. MATERIALS AND METHODS

2.1. Materials. All chemicals were purchased from Sigma-Aldrich and used as-received. Ultrapure Millipore DI water (18.2 MΩ·cm resistivity at 25°C) was used. The animal procedures were in agreement with the guidelines of the Institutional Animal Care and Use Committee of Tongji University.

2.2. Preparation of Hydrophobic Magnetic Nanoparticles. Hydrophobic Fe_3O_4 SPION were synthesized with minor modifications according to a previously published procedure.[30] Briefly, Fe $(acac)_3$ (1 mmol), 1, 2-hexadecanediol (6 mmol), oleic acid (4 mmol), oleylamino (3 mmol), and benzyl ether (12 mL) were mixed and magnetically stirred under flowing nitrogen. The mixture was heated to 200 °C for 2 h first and then to 300 °C for reflux for 1 h. The black-colored mixture was cooled to room temperature by removing the heat source. Under ambient conditions, ethanol (20 mL) was added to the mixture, and a black material was precipitated and washed with ethanol three times. The purified SPION were dried and then weighed for the following phase-transfer use.

2.3. Ultrasound-Triggered BSA/SPION Hybrid Nanoclusters. SPION/chloroform solution (8 mg/mL, 3.5 mL) was transferred into a clean syringe for injection. The weighted BSA (0.52 g) was completely dissolved in 15 mL of deionized water in a 50 mL beaker. The beaker was placed under an ultrasonic with a converter. The top of converter was placed ∼0.5 cm under the liquid level of BSA/water solution. The top of long needle on the syringe was placed next to that of the converter. Ultrasonication at 300−500 watts was pulsed every 10 seconds for a duration of 10 seconds. The SPION/chloroform solution was slowly injected into the BSA/water solution with ultrasonication. The solution in the beaker became emulsion-like after injection. Upon injection, the sample solution was quickly stirred or processed on a rotary evaporator under the reduced pressure to remove the remains of chloroform. Finally, the resulting aqueous solution was centrifuged and washed several times with deionized water to remove residual BSA.

The nanoclusters of BSA/SPION hybrid were dispersed in deionized water and dried onto carbon-coated copper grids before TEM examination on a Philips Tecnai G^2 F20 TEM operating at an acceleration voltage of 200 kV. The dispersion property of the BSA/SPION hybrid nanoclusters in solution was measured using a particle size analyzer (Nano ZS, Malvern).

2.4. In Vitro Relaxometry. The longitudinal and transverse relaxation times were measured using a 1.41 T minispec mq 60 NMR Analyzer (Bruker, Germany) at 37 °C. The in vitro MR images were obtained using a MicroMR-25 mini MRI system (Niumag Corporation, Shanghai, China). The measurement conditions were as follows: T_2-weighted sequence, multi-slice spin echo (MSE), TR/TE = 2000/20 ms, matrix acquisition = 200 × 128, NS = 2, FOV = 85 mm×85 mm, thickness = 4.9 mm, 0.55 T, 32.0 °C. Relaxivity values of r_1 and r_2 were calculated by fitting the $1/T_1$ and $1/T_2$ relaxation time (s^{-1}) versus Fe^{3+} concentration (mM) curves.

2.5. In Vivo MR Imaging. Mouse MR in vivo imaging was performed on a 1.5 T MR imaging system (GE Signa Excite twinspeed) by using a mouse coil (mouse mass ∼20 g, n = 3 for the agent of the BSA/SPION hybrid nanoclusters). Mouse was anaesthetized by pentobarbital sodium. Imaging was performed before, at various time intervals, and after intravenous injections (via the tail vein) at dose of 2.5 mg (Fe)/kg body weight of the prepared agent, using a fast spin echo imaging sequence (TR/TE = 1000/23.8 ms, FOV = 60 mm×60 mm, 7 slices, 2 mm thick, 0.5 mm space, acquisition time = 12 min 32 s). All imaging of post-processing was performed using the Advantage Workstation 4.2 (AW4.2, General Electric Healthcare).

2.6. In Vitro Cytotoxicity Assay. The in vitro cytotoxicity was measured using 3-(4,5-dimethylthiazol-2-yl)-2,5-diphenyltetrazolium bromide (MTT) assay. L929 cells growing in log phase were seeded into a 96-well cell-culture plate at 5×10^3/well and incubated for 24 h at 37 °C under 5% CO_2. DMEM supplemented with 10% FBS (fetal bovine serum) solutions of BSA/SPION hybrid nanoclusters (100 μL/well, containing 1% HEPES) at various concentrations of Fe^{3+} were added to the wells of the treatment group, and DMEM containing 1% HEPES (100 μL/well) to the negative control group, respectively. The cells were incubated for 24 h and 48 h at 37 °C under 5% CO_2. Subsequently, 10 μL of MTT (5 mg/mL) was added to each well and incubated for an additional 4 h at 37 °C under 5% CO_2. After the addition of dimethylsulfoxide (DMSO, 150 μL/well), the assay plate was allowed to stand at room temperature for 10 minutes. A Tecan Infinite M200 monochromator-based multifunction microplate reader was used to measure the OD570 (A value) of each well with background subtraction at 690 nm. The following formula was used to calculate the viability of cell growth: cell viability (%) = (mean of IA value of treatment group/mean of IA value of control) × 100.

2.7. In Vivo Biodistribution and Histology Analysis. Kunming mice (25−30 g of body weight) were purchased from the Second Military Medical University (Shanghai, China). The animal procedures were in agreement with the guidelines of the Institutional Animal Care and Use Committee of Tongji University. BSA/SPION hybrid nanoclusters at dose of 2.5 mg (Fe)/kg body weight were injected into Kunming mice (n = 3) via the tail vein.

2.7.1. In Vivo Biodistribution Studies. Major organs were removed from mice post-injected with BSA/SPION hybrid nanoclusters at the time intervals of 10 h, 48 h, 7 days, and 14 days after complete anesthesia. Three mice without injection were used as the blank control. The removed organs were pulverized and treated with nitric acid. The organ/nitric acid solutions were heated at 90 °C for eight hours and then filtered. The filtrates were ready for ICP analysis.

2.7.2. Histology Studies. Tissues were harvested from mice post-injected with BSA/SPION hybrid nanoclusters after 60 days. Mice were sacrificed after complete anesthesia. The liver, spleen, and kidney were removed and fixed in paraformaldehyde, embedded in paraffin, sectioned, and stained with

Scheme 1. Schematic Diagram Showing the Formation of BSA/SPION Hybrid Nanoclusters under Ultrasonication in a One-Pot Facile Approach

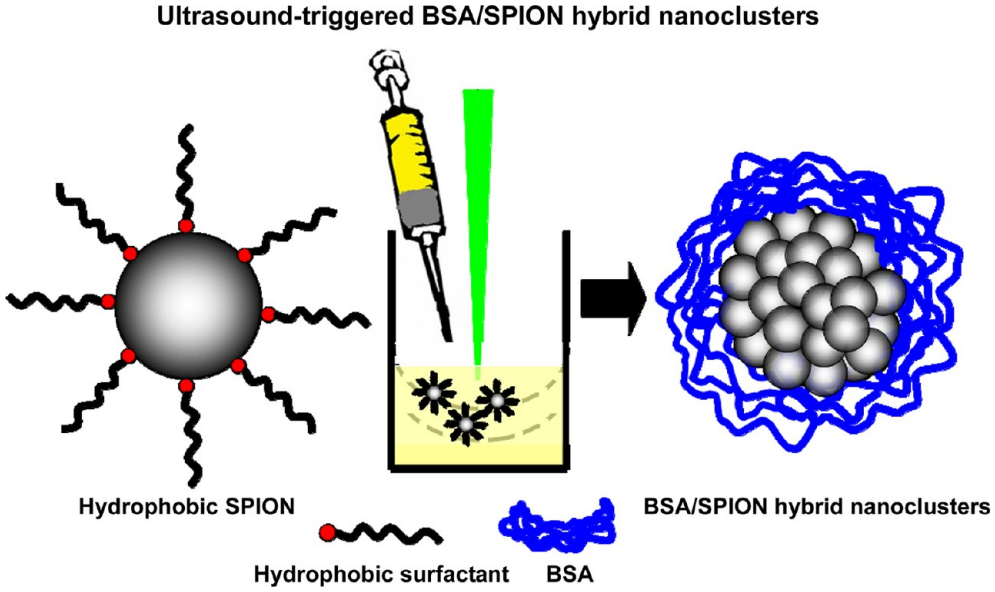

hematoxylin and eosin. The histological sections were observed under an optical microscope.

3. RESULTS AND DISCUSSIONS

3.1. Ultrasound-Triggered BSA/SPION Hybrid Nanoclusters. Proteins are commonly used biopolymers for foam formation and stabilization.[23,24,31] Their surface activity is strongly influenced by several intrinsic properties. These include conformational flexibility and stability, adaptability to environmental conditions, and distribution of hydrophobic and hydrophilic regions within their primary structure.[32] Serum albumin is one of the most widely studied proteins, that is also most abundant in plasma with a typical concentration of 5 g/100 mL. In consideration of emulsification capability and availability, BSA was selected in this study for phase-transferring of hydrophobic SPION. The roles of BSA are two-fold: one being the emulsifier between the organic and aqueous phase and the other for the coating matrix.

The general process of BSA/SPION hybrid nanoclusters involves generation of a BSA/water emulsion, triggered by ultrasonication. The injection of SPION/chloroform organic solution is synchronous followed by rotary evaporation to remove chloroform. In this process, stable "oil-in-water" emulsion is obtained via ultrasonication, in which BSA plays an important role as the emulsifier. During emulsion formation, BSA proteins diffuse to the oil/water interface and reduce the surface tension. SPION/chloroform solution, as the oil phase, is evenly distributed in the BSA/water solution (aqueous phase) as a result of ultrasonication. At the same time, the BSA macromolecules bond with the hydrophobic ligands on the surfaces of SPION. In the presence of oil-soluble SPION, ultrasonication emulsion results in SPION-clustering, which is stabilized by the BSA macromolecules. The schematic illustration of the one-pot facile SPION-clustering process is shown in Scheme 1.

In this study, the feeding ratios of BSA to SPION are found to have significant impacts on the clustering of SPION. Therefore, we systemically investigated the influence of the feeding ratios of BSA (5.3, 42.5, and 170 mg) to SPION (fixed at 10 mg) on the clustering and sizes of BSA/SPION nanoclusters. BSA/SPION hybrid nanoclusters prepared with different BSA/SPION feeding ratios were characterized by TEM (Figure 1A–D). It was found large aggregates formed in the sample of 5.3 mg of BSA. With increasing BSA, SPION can be clustered. This clustering can be achieved efficiently in the sample of 170 mg of BSA. It indicates that adequate BSA is necessary for formulation of BSA/SPION hybrid nanoclusters. The excess BSA can be efficiently removed from the formed nanoclusters by centrifugation, and the sedimentation upon centrifugation can be well redispersed in water by vortex. Figure 1D shows the TEM image of SPION as isolated cluster with dense packing at a higher magnification. As indicated by the arrow, it shows the encapsulation of SPION in BSA macromolecules. Although the emulsifying properties of the BSA, efficient clustering of SPION can not be achieved under vigorous magnetic stirring. DLS data displays a mean hydrodynamic diameter of 86.0 nm (Figure 1E). Long-term stability was monitored by measurement of hydrodynamic diameters of BSA/SPION hybrid nanoclusters at various time points (Figure 1F). It also shows they are colloidal stable.

There are two general methods for preparation of SPION: chemical coprecipitation at room temperature and thermochemical decomposition at high temperatures. Usually, the SPION prepared at high temperature has better crystallinity and relaxivity and uniform controlled size. But they are coated with hydrophobic ligands, such as oleic acid and oleylamine. These hydrophobic SPION should be endowed water-solubilization before biomedical applications.[33−35] In this study, we found a novel approach to make hydrophobic SPION water-soluble directly in the presence of BSA under ultrasonication condition. Although it is reported that immobilization BSA on iron oxide nanoparticle with different modification, such as silica, amine, and L-aspartic acid, such processes are onerous and time-consuming.[36,37] The phase-transfer in this study is the hydrophobic interactions between SPION and the internal hydrophobic sites of BSA proteins. The ultrasound-triggered clustering of SPION in the presence of BSA protein has been shown to be facile, reproducible, and

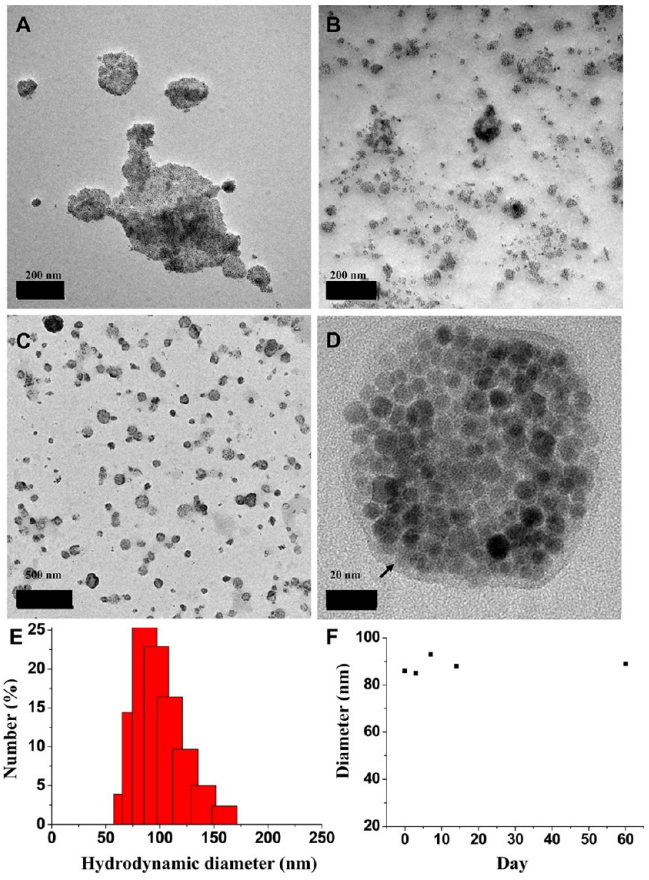

Figure 1. TEM images of BSA/SPION hybrid nanoclusters prepared with different amount of BSA: (A) 5.3 mg, (B) 42.5 mg and (C, D) 170 mg, in which SPION were all 10 mg (A-D). DLS data of BSA/SPION hybrid nanoclusters in water (E), and its colloidal hydrodynamic diameter stability in PBS by DLS (F). The samples in E and F were prepared with 170 mg of BSA and 10 mg of SPION.

rapid within 5 minutes. The as-prepared BSA/SPION hybrid nanoclusters exhibit good hydrophily, colloidal stability, and superparamagnetic behavior (Figure 2). SPION with hydrophobic ligands can be made water-soluble first by ultrasonication in the presence of BSA and then used for liver-specific MRI medical application. For biomedical applications, excellent water-solubilization is required for the in vivo contrast agent. Nanoparticles with hydrophobic surfaces are easily recognized by opsonic proteins in bloodstream.

The successful phase transfer of SPION is shown in Figure 2A. The original hydrophobic SPION are densely packed and coated/stabilized by BSA proteins (Figure 1D). The coating of BSA proteins enhances water-solubilization of the BSA/SPION hybrid nanoclusters. As a result, the clustered SPION can be dispersed in water. The dispersion is optically clear and uniform without obvious aggregates and sediments in five days (Figure 2B). The colloidal stability of BSA/SPION hybrid nanoclusters is closely related to the BSA/SPION feeding ratios. Less BSA feeding leads to sedimentation, since hydrophobic SPION are not effectively coated by BSA macromolecules (Figure 2C). The SPION remain superparamagnetic after clustering (Figures 2D and E). The saturation magnetization of the BSA/SPION hybrid nanoclusters is 38.2 emu g^{-1}. This is found to be below the theoretical value for magnetite (92−100 emu/g) due to the presence of a nonmagnetic surface layer formed by the BSA proteins.[38]

3.2. In Vitro Relaxivity Characterization of BSA/SPION Hybrid Nanoclusters. To determine the relaxivity value of BSA/SPION hybrid nanoclusters in water solution, longitudinal (T_1) and transverse proton relaxation times (T_2) were measured as a function of ferric ions concentration at 1.41T, 37°C. Different concentrations of BSA/SPION hybrid nanoclusters for relaxivity characterization were obtained by dilution with deionized water. As shown in Figure 3A, the BSA/SPION hybrid nanoclusters exhibit a high r_2 value of 600.8 s^{-1} per mM of Fe^{3+}. The T_2 relaxivity is increased dramatically with SPION clustering. This enhancement of spin−spin relaxation is associated with the distortion of the local magnetic field by the magnetic nanoparticles.[39] Similar results were found in some copolymer/SPION aggregates.[20] The r_2/r_1 value of 139.7 indicates significant advantages of the BSA/SPION hybrid nanocluster as negative MRI CAs.[40] The high relaxivity of MRI CAs is particularly useful in dose reduction, which is desirable for patients with weak organ functions.[41] For further MRI characterization, T_2-weighted MR images of BSA/SPION hybrid nanoclusters with various concentrations of Fe^{3+} were obtained. As can be seen from Figure 3B and C, the MR signal intensities of BSA/SPION hybrid nanoclusters decrease with decreasing Fe^{3+} concentration. The r_2 and r_1 relaxivities indicate that these nanoclusters behave as negative CAs.

3.3. Cytotoxicity Study of BSA/SPION Hybrid Nanoclusters. The cytotoxicity test was conducted for BSA/SPION hybrid nanoclusters on normal L929 cells. The 3-(4,5-dimethylthiazol-2-yl)-2,5-diphenyltetrazolium bromide (MTT) results show good biocompatibility of the BSA/SPION hybrid nanoclusters. The viabilities of L929 cells are over 85% (24 h) and 80% (48 h) when incubated with BSA/SPION hybrid nanoclusters at various Fe^{3+} concentrations, even at 25 μM of

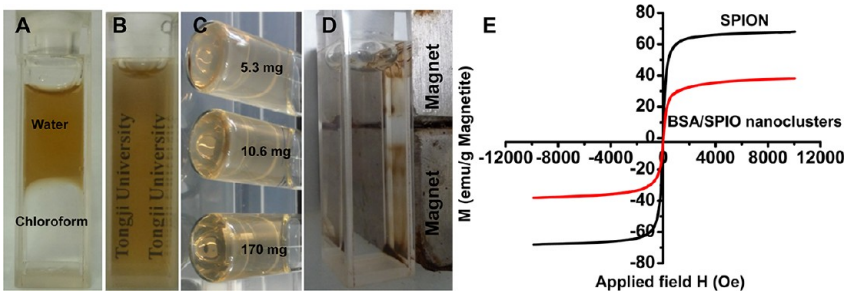

Figure 2. Optical photographs showing successful phase transfer (A); good water-solubilization (B); digital images of BSA/SPION hybrid nanoclusters prepared with different amount of BSA, 5.3, 10.6, and 170 mg, in which SPION were all 10 mg after seven-day storage at room temperature (C); the magnetic response measurement set up (D); and the magnetization curve of the BSA/SPION hybrid nanoclusters (E).

dx.doi.org/10.1021/am301301f | ACS Appl. Mater. Interfaces 2012, 4, 6479−6486

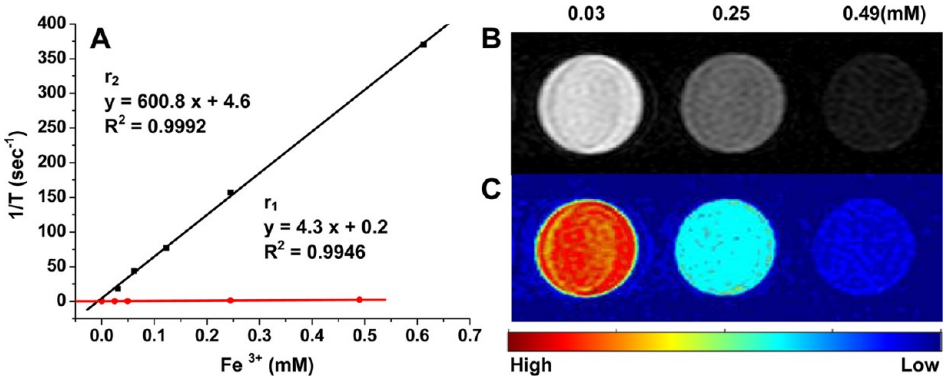

Figure 3. (A) r_1 and r_2 relaxivity curves are obtained from water solutions of BSA/SPION hybrid nanoclusters at 37°C, 1.41 T using Carr−Purcell−Meiboom−Gill (CPMG) sequence, (B) T_2-weighted, and (C) the color-mapped MR images of BSA/SPION hybrid nanoclusters (from 0.03 to 0.49 mM Fe $^{3+}$) at 32°C, 0.55 T using MSE sequence. The samples were diluted with deionized water.

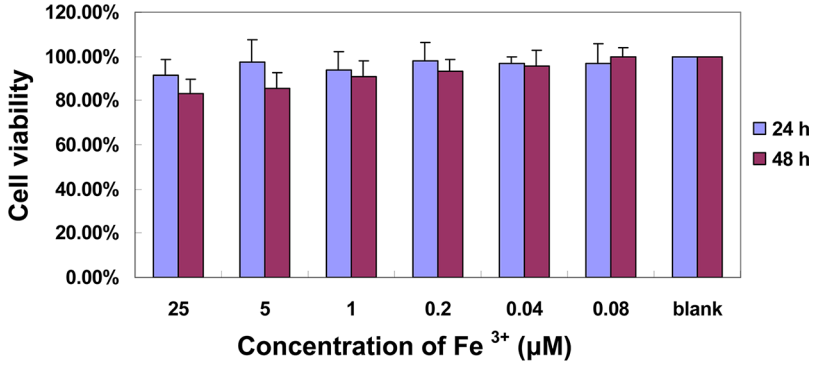

Figure 4. Viability of L929 cells incubated with BSA/SPION hybrid nanoclusters. BSA/SPION hybrid nanoclusters were incubated with L929 cells at various Fe^{3+} concentrations for 24 and 48 h and viability was measured using 3-(4,5-dimethylthiazol-2-yl)-2,5-diphenyltetrazolium bromide (MTT) assay. Viability measurements were normalized to cells grown in absence of any particles.

Fe^{3+} (Figure 4). These cytotoxicity data indicate great potential of the BSA/SPION hybrid nanoclusters for in vivo imaging.

3.4. In Vivo MRI Study and Biodistribution of BSA/SPION Hybrid Nanoclusters. Figure 5 shows liver T_2-weighted MRI acquired in vivo before and after the intravenous injections (2.5 mg (Fe)/kg body weight) of BSA/SPION hybrid nanoclusters. The first one was taken at the baseline (before injection). The first image post-injection of nanoclusters (15 min) shows good MR signal enhancement in liver. The imaging time-window of BSA/SPION hybrid nanoclusters is prolonged up to 48 h. Clinical studies have shown that the time-window for commercial Resovist contrast-enhanced MRI of the liver is between 1 and 4 days for different patients. In this study, the liver MR signal is reduced 48 h after injection of BSA/SPION hybrid nanoclusters. Axial slices of T_2-weighted MR images shows intake of nanoclusters in liver and good MR contrast in various slices of liver.

To evaluate the in vivo clearance process and biodistribution, mice were injected with 2.5 mg (Fe)/kg body weight of BSA/SPION hybrid nanoclusters via tail vein. At different time points post-injection, mice were anesthetized and sacrificed. The main organs were removed for inductively coupled plasma atomic emission spectroscopy (ICP-AES) analysis of Fe^{3+} (Figure 6). ICP analysis shows uptake and retention of BSA/SPION hybrid nanoclusters primarily in liver and spleen. The concentration of Fe^{3+} in liver decreases gradually. The BSA/SPION hybrid nanoclusters are also found in large intestine during the entire experimental period. It is noted that a high level of iron is present in kidneys 10 h post-injection. Theoretically, the injected nanoclusters with size of 86 nm can not be metabolized through glomerular filtration. This possibly indicates rapid degradation of nanoclusters into small particles/molecules.

There are two primary routes of clearance of nanoparticles from body. One is the renal filtration with excretion into urine; and the other is hepatobiliary (HB) processing with excretion into bile.[42] Clearance of nanoparticles is determined by many factors, including particle size/shape, surface ligand, and surface charge density. Larger particles are more easily trapped by liver and the RES system.[43] The clearance studies on silica nanoparticles of 20−25 nm suggest an initial uptake of the nanoparticles by the RES system, followed by their gradual degradation and excretion via the HB mechanism over a period of 15 days.[44] Liu et al. reported the near-complete clearance of single-walled carbon nanotubes (SWNTs), functionalized with polyethylene-glycol (PEG) from mice via the HB and renal pathways in approximately 2 months.[45] In this study, the clearance route of the BSA/SPION hybrid nanoclusters are mainly via HB processing with excretion into bile over a period of 14 days. This has been investigated and verified by ICP analysis.

3.5. Histology Analysis. To further investigate toxicity of BSA/SPION hybrid nanoclusters in vivo, histological assessment of tissues was conducted to determine tissue damage, inflammation, or lesions from toxic exposure. Analysis was performed on the tissues obtained from the harvested organs to assess signs of potential toxicity. The histology analysis can be carried out by administration of the BSA/SPION hybrid

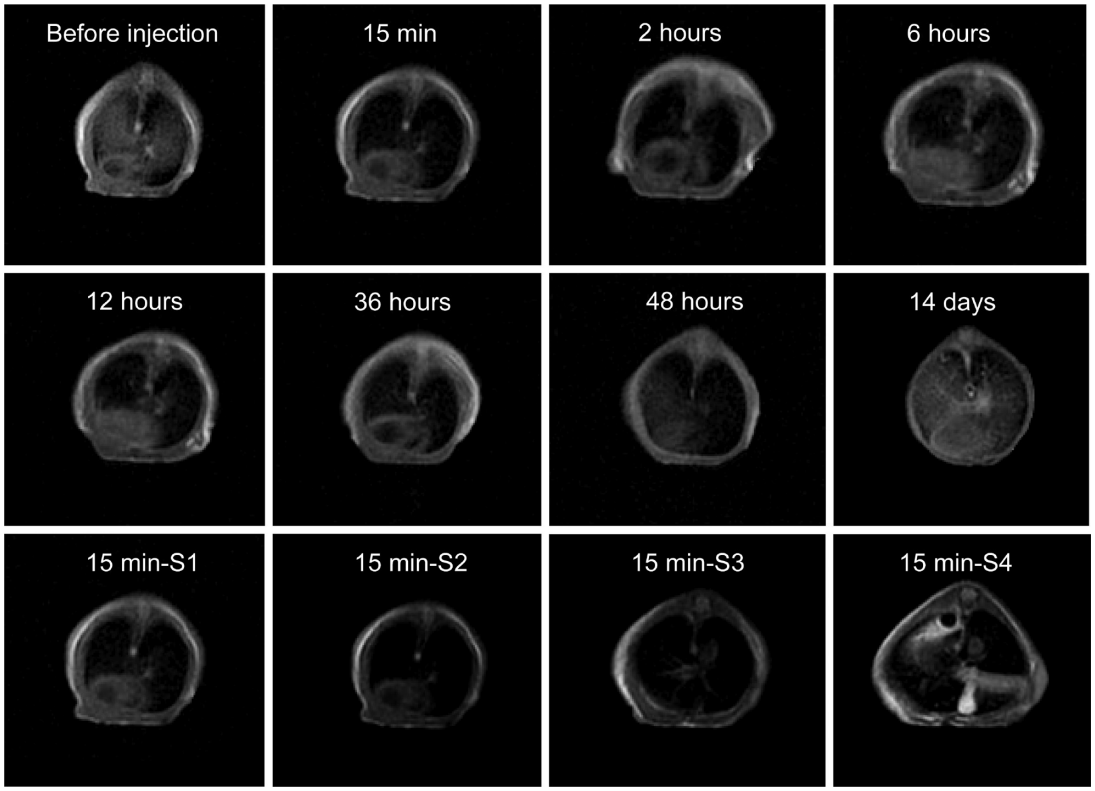

Figure 5. Mouse liver T_2-weighted MRI images at different time points before and after administration of BSA/SPION hybrid nanoclusters, and axial slices of T_2-weighted MR images of BSA/SPION hybrid nanoclusters in liver at 15 min post-injection. All images were obtained at dose of 2.5 mg (Fe)/kg body weight.

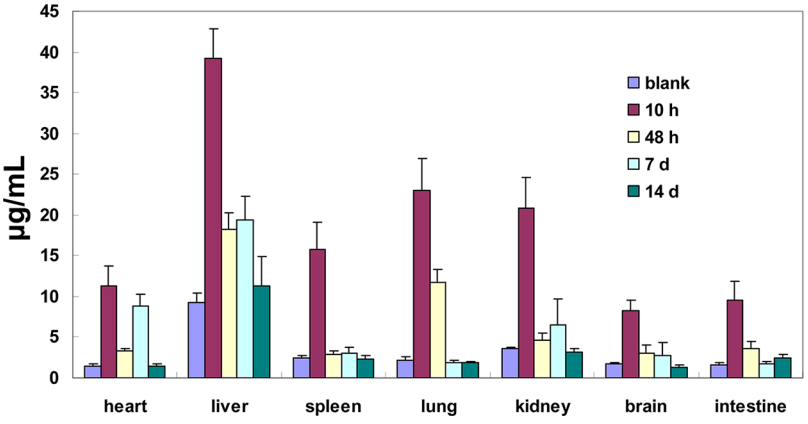

Figure 6. Biodistributions in organs of mice with intravenous injection of BSA/SPION hybrid nanoclusters (2.5 mg (Fe)/kg body weight) at different time points. Error bars are based on three administrated mice.

nanoclusters into mice in subsequent two-month period. In this study, three most possible organs (liver, spleen, and kidney) were chosen for in vivo toxicity test. Considering the similarities of pharmacokinetics of nanoclusters in both liver and lung, liver was chosen for histology analysis for its higher uptake. Spleen was also chosen for its nature of filtering foreign objects as an organ of reticuloendothelial system (RES). Kidney was selected for studying the clearance process of the nanoclusters. As can be seen in Figure 7, the structures of organs from the exposed mice were normal, hardly different from those of the control group. Hepatocytes in the liver and spleen samples appeared normal, and there were no inflammatory infiltrates. The glomerulus structure could be distinguished easily in the kidney samples. No necrosis was found in any of the groups. The observed biocompatibility is attributable to the green chemical synthesis and BSA biomolecular coating.

4. CONCLUSIONS

In conclusion, a new approach has been developed for the preparation of superparamagnetic BSA/SPION hybrid nanoclusters as negative liver-specific MRI CAs. The hydrophobic SPION are efficiently clustered in the presence of BSA macromolecules under ultrasonication condition. The resulting BSA/SPION hybrid nanoclusters with uniform size of ~86 nm show excellent colloidal stability and good biocompatibility. The high value of r_2/r_1 ratio (139.7) obtained from the BSA/SPION hybrid nanoclusters is favorable for T_2 relaxation

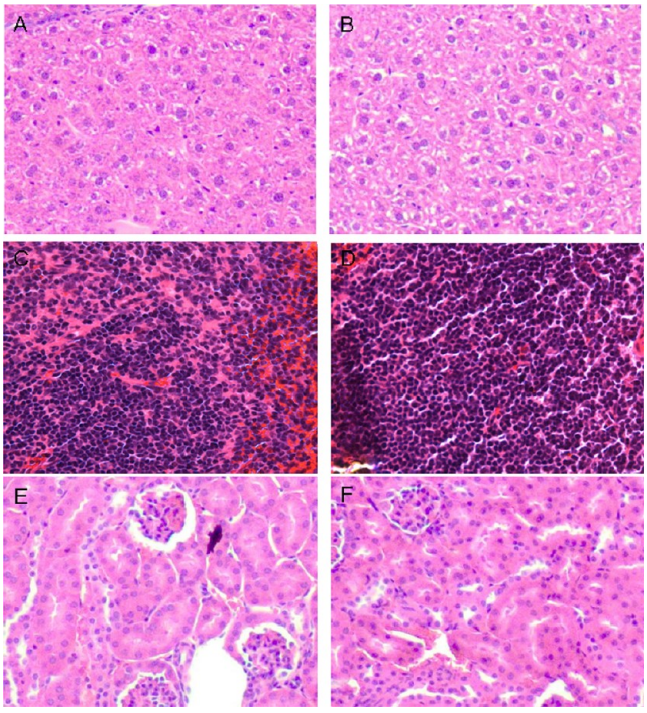

Figure 7. Hematoxylin and eosin-stained tissue sections from mice receiving no injection (A, C, and E) and injected with BSA/SPION hybrid nanoclusters 60 days post-injection (B, D, and F). Tissues were harvested from liver (A, B), spleen (C, D), and kidney (E, F).

enhancement. The liver-specific MRI time-window is prolonged to up to 48 h. Biodistribution results indicate gradual clearance of the BSA/SPION hybrid nanoclusters from body via HB processing. No obvious toxicity on normal cells is found from in vitro MTT assay and in vivo toxicity studies. It is, therefore, the conclusion of this study that the BSA/SPION hybrid nanoclusters will present great potential in liver-specific MRI.

AUTHOR INFORMATION

Corresponding Author

*E-mail: bingbozhang@tongji.edu.cn (B.Z.); donglu.shi@uc.edu (D.S.). Tel: (+)86-21-65983706-819 (D.S.). Fax: (+) 86-21-65983706-0 (D.S.).

Notes

The authors declare no competing financial interest.

ACKNOWLEDGMENTS

This work was supported by the National Natural Science Foundation of China (51003078, 81171393, 81271629), the Nanotechnology Program of Shanghai Science & Technology Committee (11 nm0504500), Program for Outstanding Young Teachers in Tongji University, and the Fundamental Research Funds for the Central Universities.

REFERENCES

(1) Kressel, H. Y. *Radiat. Med.* **1983**, *1*, 197−204.
(2) Lanza, G. M.; Winter, P. M.; Caruthers, S. D.; Morawski, A. M.; Schmieder, A. H.; Crowder, K. C.; Wickline, S. A. *J. Nucl. Cardiol.* **2004**, *11*, 733−743.
(3) Mezrich, R. S. *Med. Device Technol.* **1990**, *1*, 46−50.
(4) Leach, J. L.; Holland, S. K. *Pediatr. Radiol.* **2010**, *40*, 31−49.
(5) Kangarlu, A. *Neuroimaging Clin. N Am.* **2009**, *19*, 113−128.
(6) Hocaoglu, Y.; Roosen, A.; Herrmann, K.; Tritschler, S.; Stief, C.; Bauer, R. M. *BJU Int.* **2012**, *109*, 234−239.
(7) Reichenbach, J. R. *Neuroimage* **2012**, *62*, 1311−1315.
(8) Weinmann, H. J.; Brasch, R. C.; Press, W. R.; Wesbey, G. E. *AJR, Am. J. Roentgenol.* **1984**, *142*, 619−624.
(9) Penfield, J. G.; Reilly, R. F. *Nat. Clin. Pract. Nephrol.* **2007**, *3*, 654−668.
(10) Arsalani, N.; Fattahi, H.; Laurent, S.; Burtea, C.; Vander Elst, L.; Muller, R. N. *Contrast Media Mol. Imaging* **2012**, *7*, 185−194.
(11) Wang, Q. B.; Han, Y.; Jiang, T. T.; Chai, W. M.; Chen, K. M.; Liu, B. Y.; Wang, L. F.; Zhang, C. F.; Wang, D. B. *Eur. Radiol.* **2011**, *21*, 1016−1025.
(12) Cheng, F. Y.; Su, C. H.; Yang, Y. S.; Yeh, C. S.; Tsai, C. Y.; Wu, C. L.; Wu, M. T.; Shieh, D. B. *Biomaterials* **2005**, *26*, 729−738.
(13) Song, Y. J.; Wang, R. X.; Rong, R.; Ding, J.; Liu, J.; Li, R. S.; Liu, Z. H.; Li, H.; Wang, X. Y.; Zhang, J.; Fang, J. *Eur. J. Inorg. Chem.* **2011**, 3303−3313.
(14) Poselt, E.; Kloust, H.; Tromsdorf, U.; Janschel, M.; Hahn, C.; Masslo, C.; Weller, H. *ACS Nano* **2012**, *6*, 1619−1624.
(15) Berret, J. F.; Schonbeck, N.; Gazeau, F.; El Kharrat, D.; Sandre, O.; Vacher, A.; Airiau, M. *J. Am. Chem. Soc.* **2006**, *128*, 1755−1761.
(16) Ai, H.; Flask, C.; Weinberg, B.; Shuai, X.; Pagel, M. D.; Farrell, D.; Duerk, J.; Gao, J. M. *Adv. Mater.* **2005**, *17*, 1949−1952.
(17) Xie, X. A.; Zhang, C. F. *J. Nanomater.* **2011**, 152524−152527.
(18) Nasongkla, N.; Bey, E.; Ren, J. M.; Ai, H.; Khemtong, C.; Guthi, J. S.; Chin, S. F.; Sherry, A. D.; Boothman, D. A.; Gao, J. M. *Nano Lett.* **2006**, *6*, 2427−2430.
(19) Riess, G. *Prog. Polym. Sci.* **2003**, *28*, 1107−1170.
(20) Lu, J.; Ma, S. L.; Sun, J. Y.; Xia, C. C.; Liu, C.; Wang, Z. Y.; Zhao, X. N.; Gao, F. B.; Gong, Q. Y.; Song, B.; Shuai, X. T.; Ai, H.; Gu, Z. W. *Biomaterials* **2009**, *30*, 2919−2928.
(21) Lee, D.-E.; Kim, A. Y.; Yoon, H. Y.; Choi, K. Y.; Kwon, I. C.; Jeong, S. Y.; Park, J. H.; Kim, K. *J. Mater. Chem.* **2012**, *22*, 10444−10447.
(22) Kim, B. S.; Qiu, J. M.; Wang, J. P.; Taton, T. A. *Nano Lett.* **2005**, *5*, 1987−1991.
(23) Singh, A. V.; Bandgar, B. M.; Kasture, M.; Prasad, B. L. V.; Sastry, M. *J. Mater. Chem.* **2005**, *15*, 5115−5121.
(24) Singh, A. V.; Patil, R.; Kasture, M. B.; Gade, W. N.; Prasad, B. L. V. *Colloids Surf., B* **2009**, *69*, 239−245.
(25) Goodman, D. S. *J. Am. Chem. Soc.* **1958**, *80*, 3892−3808.
(26) Roda, A.; Cappelleri, G.; Aldini, R.; Roda, E.; Barbara, L. *J. Lipid Res.* **1982**, *23*, 490−495.
(27) Brodersen, R. *J. Biol. Chem.* **1979**, *254*, 2364−2369.
(28) Westphal, U.; Harding, G. B. *Biochim. Biophys. Acta* **1973**, *310*, 518−527.
(29) Daughaday, W. H. *Physiol. Rev.* **1959**, *39*, 885−902.
(30) Sun, S.; Zeng, H.; Robinson, D. B.; Raoux, S.; Rice, P. M.; Wang, S. X.; Li, G. *J. Am. Chem. Soc.* **2004**, *126*, 273−279.
(31) Wilde, P. J. *Curr. Opin. Colloid Interface Sci.* **2000**, *5*, 176−181.
(32) Halling, P. J. *Crit. Rev. Food Sci. Nutr.* **1981**, *15*, 155−203.
(33) Laurent, S.; Forge, D.; Port, M.; Roch, A.; Robic, C.; Vander Elst, L.; Muller, R. N. *Chem. Rev.* **2008**, *108*, 2064−2110.
(34) Gao, J.; Gu, H.; Xu, B. *Acc. Chem. Res.* **2009**, *42*, 1097−1107.
(35) Sun, S.; Zeng, H. *J. Am. Chem. Soc.* **2002**, *124*, 8204−8205.
(36) Yu, C. H.; Al-Saadi, A.; Shih, S.-J.; Qiu, L.; Tam, K. Y.; Tsang, S. C. *J. Phys. Chem. C* **2008**, *113*, 537−543.
(37) Mikhaylova, M.; Kim, D. K.; Berry, C. C.; Zagorodni, A.; Toprak, M.; Curtis, A. S. G.; Muhammed, M. *Chem. Mater.* **2004**, *16*, 2344−2354.
(38) Sondjaja, R.; Hatton, T. A.; Tam, M. K. C. *J. Magn. Magn. Mater.* **2009**, *321*, 2393−2397.
(39) Josephson, L.; Lewis, J.; Jacobs, P.; Hahn, P. F.; Stark, D. D. *Magn. Reson. Imaging* **1988**, *6*, 647−653.
(40) Burtea, C.; Laurent, S.; Vander Elst, L.; Muller, R. N. *Handb. Exp. Pharmacol.* **2008**, 135−165.
(41) Secchi, F.; Di Leo, G.; Papini, G. D.; Giacomazzi, F.; Di Donato, M.; Sardanelli, F. *Eur. J. Radiol.* **2011**, *80*, 96−102.

(42) Zhu, W.; Artemov, D. *Contrast Media Mol. Imaging* **2011**, *6*, 61−68.
(43) Souris, J. S.; Lee, C. H.; Cheng, S. H.; Chen, C. T.; Yang, C. S.; Ho, J. A.; Mou, C. Y.; Lo, L. W. *Biomaterials* **2010**, *31*, 5564−5574.
(44) Kumar, R.; Roy, I.; Ohulchanskky, T. Y.; Vathy, L. A.; Bergey, E. J.; Sajjad, M.; Prasad, P. N. *ACS Nano* **2010**, *4*, 699−708.
(45) Liu, Z.; Davis, C.; Cai, W. B.; He, L.; Chen, X. Y.; Dai, H. J. *Proc. Natl. Acad. Sci. U. S. A.* **2008**, *105*, 1410−1415.